V. PIERLOT and M. VAN DROOGENBROECK. **Analysis of a robot positioning system based on a rotating receiver, beacons, and coded signals**. In *Proceedings of the European Signal Processing Conference (EUSIPCO)*, Barcelona, Spain, pages 1766-1770, August 2011.

ANALYSIS OF A ROBOT POSITIONING SYSTEM BASED ON A ROTATING RECEIVER, BEACONS, AND CODED SIGNALS

V. Pierlot and M. Van Droogenbroeck

INTELSIG Laboratory, Montefiore Institute, University of Liège, Belgium

ABSTRACT

Positioning is a fundamental issue in mobile robot applications that can be achieved in multiple ways. Among these methods, triangulation with active beacons is widely used, robust, accurate, and flexible. In this paper, we analyze the performance of an original system, introduced in one of our previous papers, that comprises a rotating receiver and beacons that send an On-Off Keying modulated infrared signal. The probability density functions of the measured angles are established and discussed. In particular, it is shown that the proposed estimator is a non biased estimator of the beacon angular position. We also evaluate the theoretical results by means of both a simulator and measurements.

1. INTRODUCTION

In a previous paper [3], we have presented an original system for robot positioning used during the Eurobot contest since 2008. The system comprises a turning turret that measures angles based on signals sent by several infrared beacons (see Figure 1 for an illustration of the Eurobot setup). These angles, denoted α_i, are combined, during a triangulation calculus, to compute the current position of a mobile robot in a 2D plane [1, 4]. In order to identify a beacon and to increase the robustness against noise, each beacon sends a unique binary sequence encoded as an On-Off Keying (OOK) amplitude modulated signal.

In this paper, we evaluate the error made on measured angles resulting from the coding of signals sent by the beacons. As explained in [3], the modulation of the 455 [kHz] carrier beacon signal makes it possible to identify beacons but, as a drawback, introduces errors that occur when no signal is sent, that is during an OFF period of the sequence. In the following, we address the issues raised by the use of an OOK modulation mechanism. An angle estimator is proposed and we characterize its performance by means of a simulator and experiments.

The paper is organized as follows. In Section 2, we first briefly present the principle of the original positioning system described in [3]. Section 3 discusses the origin of the errors. In Section 4, we propose several estimators and compute the probability density functions of the measured angles. Then we present and discuss the experimental results in Section 5, and conclude the paper in Section 6.

2. ANGLE MEASUREMENT PRINCIPLE

The system described in [3] is an angle measurement sensor based on fixed infrared beacons, a rotating turret turning at a constant speed ω, and an infrared receiver (TSOP7000). Each beacon continuously emits an infrared (IR) signal in all directions in a horizontal 2D plane. Let us denote by ϕ the current angular position of the receiver. As the turret turns at a constant speed, the angular position ϕ is directly proportional to time

$$\phi(t) = \omega t. \tag{1}$$

As a result, we can either talk about time or angular position indifferently. In fact, the processing unit of the positioning system measures times corresponding to angles thanks to eq. (1). Although the system measures times, we prefer to think in terms of angles, because it is more intuitive for the developments.

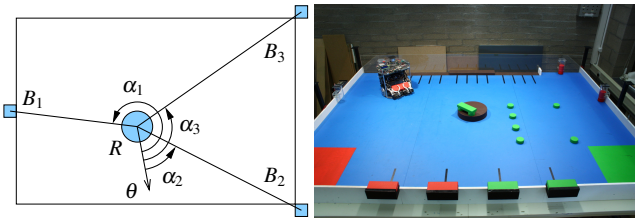

Figure 1: Left-hand side drawing: triangulation setup in the 2D plane. The circle and the small squares represent the mobile robot (R) and the beacons (B_i) respectively. α_i are the angle measurements for each B_i, relatively to the robot reference orientation θ. Right-hand side image: playing field of the EUROBOT contest 2009.

The receiver has a limited field of view and, consequently, the amount of infrared power collected at the receiver, denoted by $P_{IR}(\phi)$, depends on the angle. Moreover, this power depends on the power emitted by the beacon and the distance between the beacon and the receiver. The exact shape of $P_{IR}(\phi)$ depends on the hardware used (receiver, optical components and geometry of turret) and, unfortunately, the information available at the receiver output is too sparse to derive a precise curve. Indeed, we have only access to the demodulated signal and no information about power is available. Therefore, we make some basic assumptions on $P_{IR}(\phi)$. Figure 2 shows a possible curve for $P_{IR}(\phi)$ (top curve). The shape of this curve has not much importance in this study but is supposed to increase from a minimum to a maximum and then to decrease from this maximum to the minimum. In the following theoretical developments, we make three important assumptions about the curve and the detection process itself:

1. The maximum occurs at an angle which is the angular position of the beacon, denoted ϕ_b. In other words, we have, for any angle ϕ
$$P_{IR}(\phi) \leq P_{IR}(\phi_b). \tag{2}$$
2. The curve is also supposed to be symmetric around the maximum since the turret and all optical components are symmetric. Therefore, we consider that
$$P_{IR}(\phi_b - \phi) = P_{IR}(\phi_b + \phi). \tag{3}$$
3. Finally, we suppose that the receiver reacts to $0 \rightarrow 1$ (raising) and $1 \rightarrow 0$ (falling) transitions at the same infrared power threshold P_{th}, respectively at an angle ϕ_r and ϕ_f
$$P_{IR}(\phi_r) = P_{IR}(\phi_f) = P_{th}. \tag{4}$$

From eq. (3) and (4), we can see that $\phi_b - \phi_r = \phi_f - \phi_b$ and, consequently, that

$$\phi_b = \frac{\phi_r + \phi_f}{2}. \tag{5}$$

If the beacons are assumed to send a non modulated IR signal (that is, a pure 455 [kHz] sine wave), the measurement of the angular position of a given beacon works as follows: while the turret

V. PIERLOT and M. VAN DROOGENBROECK. **Analysis of a robot positioning system based on a rotating receiver, beacons, and coded signals**. In *Proceedings of the European Signal Processing Conference (EUSIPCO)*, Barcelona, Spain, pages 1766-1770, August 2011.

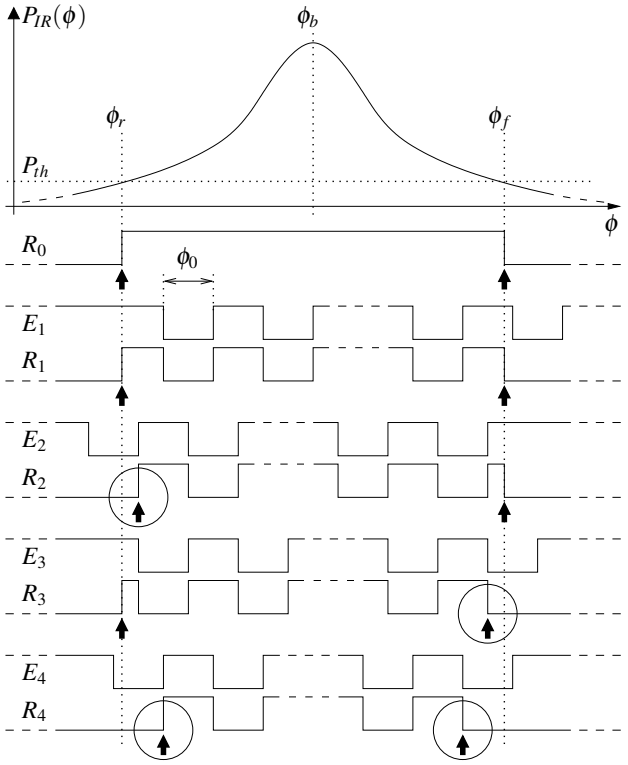

Figure 2: The upper curve $P_{IR}(\phi)$ is the infrared power collected at the receiver while the turret is turning. E_i are examples of emitted signals from the beacons. R_i are the corresponding received signals at the receiver output. R_0 is a special case corresponding to a non modulated infrared carrier (no blank periods). The black arrows represent the measured values respectively for Φ_r to the left (first *Rising* edge) and for Φ_f to the right (last *Falling* edge). The encircled arrows emphasize errors committed on Φ_r or Φ_f.

is turning, the receiver begins to "see" the IR signal from that beacon when the threshold P_{th} is crossed upwards ($0 \rightarrow 1$ transition). The receiver will continue to receive that signal until P_{th} is crossed downwards ($1 \rightarrow 0$ transition). The receiver output is depicted as R_0 in Figure 2. The estimator used for ϕ_r is the angular position of the first rising edge at the receiver output; the estimator is denoted by Φ_r hereafter. The estimator used for ϕ_f is the angular position of the last falling edge at the receiver output; it is denoted by Φ_f. These estimators are represented by the black arrows in Figure 2. The estimator Φ_b of the beacon angular position ϕ_b derives from eq. (5)

$$\Phi_b = \frac{\Phi_r + \Phi_f}{2}, \tag{6}$$

where Φ_r, Φ_f and Φ_b are random variables.

Until now, we have considered that the IR signal is not modulated. But the situation is different because the IR receiver gets an On-Off Keying amplitude modulation of a 455 [kHz] carrier frequency, otherwise it would not be possible to distinguish between beacons, and this introduces some errors.

3. SOURCE OF THE ERRORS

Even if we would use a pure 455 [kHz] carrier, noise or other irrelevant IR signals could produce erroneous transitions at the receiver output, and consequently erroneous Φ_r or Φ_f. In order to identify the different beacons and to be robust against noise, each beacon sends its own coded signal. These coded signals solve issues mentioned previously but introduce a new error, as detailed hereafter.

The receiver gets an OOK amplitude modulated signal. It means that the information can be represented only by the presence of the carrier (denoted by a 1 or ON period) or the absence of the carrier (denoted by a 0 or OFF period). The coding of the beacon signals will inevitably introduce 0's in the emitted sequences. Let us now examine the effects of the code on the detection time. If a beacon emits a 1 while it enters into the receiver field of view, there is no error on Φ_r, meaning that $\Phi_r = \phi_r$. However, if a beacon emits a 0 while it enters the receiver field of view, there is an error on Φ_r because no signal produces a $0 \rightarrow 1$ transition at the receiver output. In fact the transition occurs later ($\Phi_r \geq \phi_r$), at the next 1. The same consideration applies to Φ_f, except that the $1 \rightarrow 0$ transition could occur sooner ($\Phi_f \leq \phi_f$).

Such situations are illustrated in Figure 2. We first represent the output of the receiver for a non modulated carrier, R_0. In that case there are no errors on the transition times because the beacon constantly emits 1's. The four other cases represent the output of the receiver for four different situations using an arbitrary code. The first case (R_1) does not generate errors because P_{th} is reached twice while the beacon emits a 1. The second case (R_2) generates an error on Φ_r only because P_{th} is reached in a 0 period. The third case (R_3) generates an error on Φ_f only and the fourth case (R_4) generates an error on both Φ_r and Φ_f. From Figure 2, one can see that the receiver output R_i for an emitted signal E_i is the logical AND between E_i and R_0. Now suppose that the OFF periods of a sequence have the same duration, denoted by ϕ_0 (this is the case by design). The worst case for Φ_r occurs when an OFF period starts at an angle $\phi = \phi_r$, delaying the next transition at an angle $\Phi_r = \phi_r + \phi_0$. The same reasoning applies to Φ_f when an OFF period begins at an angle $\phi = \phi_f - \phi_0$. In both cases, the maximum absolute error on Φ_r or Φ_f is equal to ϕ_0. These are the worst cases but there are many combinations of these two errors. The next Section evaluates the probability density functions of the estimated angles.

4. ERROR ANALYSIS

In order to determine the underlying statistics of the errors, we have to analyze the influence of the code on the detection times. In this section, we determine the probability density functions (*PDFs*) of several random variables: the angle Φ_r when the beacon enters the field of view of the receiver, the angle Φ_f when the beacon leaves the field of view of the receiver, and the angular position of the beacon Φ_b, according to eq. (6).

4.1 Notations

In the following, we use these notations:

- p_0, p_1: the probability to get a "0" or a "1" respectively at the IR power threshold (rising or falling edge), that is the frequency of 0 (or 1) symbols in the code. As usual, we have $p_0 + p_1 = 1$.
- T_0: the duration of a blank period (0 symbol) in a code. The only requirement in this study is that the blank periods of a code must all have the same duration.
- ϕ_0: the angle corresponding to the blank period T_0

$$\phi_0 = \omega T_0. \tag{7}$$

Note that, in our design, we have: $p_0 = 1/6$, $T_0 = 30.8\,[\mu s]$, $\omega = 10\,[2\pi/s]$, and $\phi_0 = 0.111\,[degree]$.

The Uniform *PDF*, used later, is defined as

$$U_{(a,b)}(x) \quad = \quad \begin{cases} \frac{1}{b-a} & \text{if } a \leq x \leq b, \\ 0 & \text{otherwise} \end{cases} \tag{8}$$

whose variance is $\frac{(b-a)^2}{12}$. The symmetric Triangular *PDF* is

$$T_{(a,b)}(x) \quad = \quad \begin{cases} \frac{2}{b-a} - \frac{2|2x-a-b|}{(b-a)^2} & \text{if } a \leq x \leq b, \\ 0 & \text{otherwise} \end{cases} \tag{9}$$

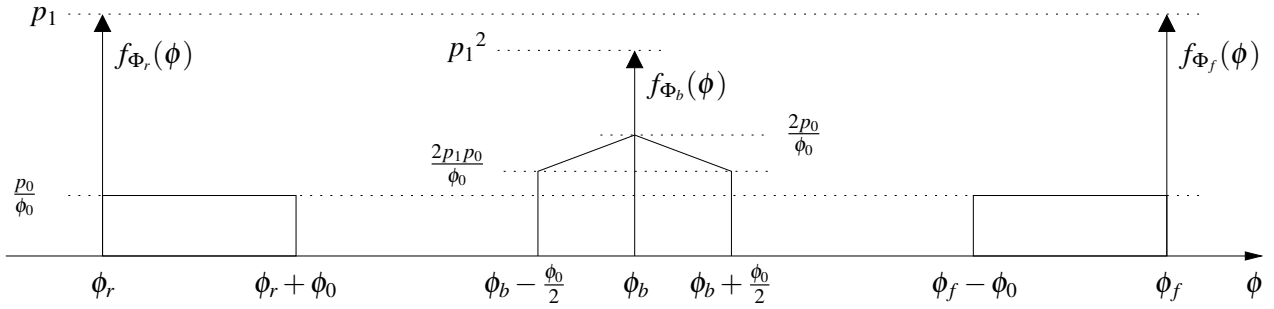

Figure 3: Probability density functions of Φ_r (left), Φ_f (right) and Φ_b (center) in the case of independent Φ_r and Φ_f.

where $|x|$ denotes the absolute value of x and whose variance is $\frac{(b-a)^2}{24}$. The mean of these two *PDFs* is given by $\frac{a+b}{2}$. Note that with these notations, and if $b-a=d-c$, we have [2, page 137]

$$U_{(a,b)}(x) \otimes U_{(c,d)}(x) = T_{(a+c,b+d)}(x), \tag{10}$$

where $\otimes$ denotes the convolution product.

4.2 Probability density function of Φ_r

Errors on Φ_r originate if a beacon is emitting a 0 symbol while entering the receiver's field of view. Assuming time stationarity and as there is no synchronization between the beacons and the receiver, the probability to determine the correct angle, that is to have $\Phi_r = \phi_r$, while the beacon enters the field of view of the receiver is given by p_1. On the other hand, when the beacon emits a 0, the value of Φ_r is uniformly distributed between ϕ_r and $\phi_r+\phi_0$. Therefore, if we define $\delta(x)$ as the DIRAC delta function, then the *PDF* of Φ_r is given by

$$f_{\Phi_r}(\phi) = p_1\delta(\phi-\phi_r) + p_0 U_{(\phi_r,\phi_r+\phi_0)}(\phi) \tag{11}$$

for $\phi \in [-\pi, \pi]$. The mean and variance of Φ_r are

$$\mu_{\Phi_r} = \phi_r + p_0\frac{\phi_0}{2}, \tag{12}$$

$$\sigma^2_{\Phi_r} = p_0\frac{\phi_0^2}{3} - p_0^2\frac{\phi_0^2}{4}. \tag{13}$$

4.3 Probability density function of Φ_f

Because the configuration is symmetric when the source leaves the field of view of the receiver, a similar result yields for Φ_f

$$f_{\Phi_f}(\phi) = p_1\delta(\phi-\phi_f) + p_0 U_{(\phi_f-\phi_0,\phi_f)}(\phi), \tag{14}$$

for $\phi \in [-\pi, \pi]$. The mean and variance of Φ_f are

$$\mu_{\Phi_f} = \phi_f - p_0\frac{\phi_0}{2}, \tag{15}$$

$$\sigma^2_{\Phi_f} = p_0\frac{\phi_0^2}{3} - p_0^2\frac{\phi_0^2}{4}. \tag{16}$$

4.4 Characteristics of the Φ_r and Φ_f estimators

The *PDFs* of Φ_r and Φ_f are drawn in Figure 3. The expectations of Φ_r and Φ_f have a bias given by $\pm p_0\frac{\phi_0}{2}$ respectively (see eq. (12) and (15)). The bias is proportional to the blank period ϕ_0 and the proportion of 0's in a code p_0. The variances of Φ_r and Φ_f are equal.

4.5 Characteristics of the estimator Φ_b

The aim of the system being to estimate the beacon angular position ϕ_b, we are now interested in finding the mean and variance of Φ_b. Generally the mean and variance of a random variable are calculated with the help of the *PDF*. In the case of Φ_b, it is not necessary since the estimator is a function of Φ_r and Φ_f (eq. (6)), whose *PDFs* are known. Let us first consider the mean of Φ_b

$$\begin{aligned}\mu_{\Phi_b} &= \frac{E\{\Phi_r\}+E\{\Phi_f\}}{2} = \frac{\left(\phi_r + p_0\frac{\phi_0}{2}\right)+\left(\phi_f - p_0\frac{\phi_0}{2}\right)}{2}, \\ &= \frac{\phi_r+\phi_f}{2} = \phi_b.\end{aligned} \tag{17}$$

As can be seen, the mean of Φ_b is unbiased, despite that both the entering angle Φ_r and leaving angle Φ_f estimators are biased. This justifies the construction of a symmetric receiver and the use of that estimator.

Let us now derive the variance of Φ_b

$$\sigma^2_{\Phi_b} = var\left\{\frac{\Phi_r+\Phi_f}{2}\right\} = \frac{var\{\Phi_r+\Phi_f\}}{4}. \tag{18}$$

If Φ_r and Φ_f are uncorrelated, we have [2, page 155]

$$\sigma^2_{\Phi_b} = \frac{var\{\Phi_r\}+var\{\Phi_f\}}{4} = \frac{\sigma^2_{\Phi_r}}{2} = \frac{\sigma^2_{\Phi_f}}{2}, \tag{19}$$

since $\sigma^2_{\Phi_r} = \sigma^2_{\Phi_f}$. This could also have been derived from the *PDF* of Φ_b, that is given by, in the case of independent Φ_r and Φ_f

$$\begin{aligned}f_{\Phi_b}(\phi) &= p_1^2\delta(\phi-\phi_b) \\ &+ 2p_1p_0 U_{(\phi_b-\frac{\phi_0}{2},\phi_b+\frac{\phi_0}{2})}(\phi) \\ &+ p_0^2 T_{(\phi_b-\frac{\phi_0}{2},\phi_b+\frac{\phi_0}{2})}(\phi).\end{aligned} \tag{20}$$

This result is obtained by convolving the *PDFs* of Φ_r and Φ_f [2, page 136], using eq. (10) and rescaling the result by using these properties [2]: 1) if $Y=\alpha X$, then $f_Y(y) = \frac{1}{|\alpha|}f_X\left(\frac{y}{\alpha}\right)$, and 2) $\delta(\alpha x) = \frac{1}{|\alpha|}\delta(x)$. This density is also depicted in Figure 3 (center). However, the non correlation or independence of Φ_r and Φ_f are questionable in our case as explained below.

To compute eq. (19) and (20), we have assumed that Φ_r and Φ_f were uncorrelated or independent. But, of course, the codes are deterministic and not random. In fact, depending on the code and the field of view $\phi_f-\phi_r$, it is not certain that an error is possible on Φ_r and Φ_f simultaneously (because the durations between blank periods are fixed and known). Depending on the receiver field of view, the rotating speed and the code, four situations are possible: (1) no error is encountered, (2) an error occurs for Φ_r only, (3) an error occurs for Φ_f only, and (4) an error occurs for both angles.

These remarks show that the Φ_r and Φ_f variables are linked, and that the nature of the relationship depends on the field of view and the coding scheme. To establish this relationship, we should analyze, in full details, the four previous cases in function of the field of view and the different codes. However, the mean of Φ_b is always given by eq. (17), and despites the relationship between Φ_r and Φ_f, Φ_b remains unbiased. To the contrary, the variance of Φ_b is no longer given by eq. (19) when Φ_r and Φ_f are correlated. Fortunately, it is possible to derive an upper bound for $\sigma^2_{\Phi_b}$. We can expand eq. (18) in [2, page 155]

$$\sigma^2_{\Phi_b} = \frac{\sigma^2_{\Phi_r} + \sigma^2_{\Phi_f} + 2C\{\Phi_r, \Phi_f\}}{4}, \tag{21}$$

where $C\{\Phi_r, \Phi_f\}$ is the covariance of Φ_r and Φ_f. Since, the square of the covariance is upper bounded [2, page 153]

$$C^2\{\Phi_r, \Phi_f\} \leq \sigma^2_{\Phi_r}\sigma^2_{\Phi_f}, \tag{22}$$

and that $\sigma^2_{\Phi_r} = \sigma^2_{\Phi_f}$, we can give the upper bound of $\sigma^2_{\Phi_b}$ by using eq. (21) and (22), resulting in

$$\sigma^2_{\Phi_b} \leq \sigma^2_{\Phi_r} = p_0\frac{\phi_0^2}{3} - p_0^2\frac{\phi_0^2}{4}. \tag{23}$$

5. EXPERIMENTAL RESULTS

The expression of the upper bound of $\sigma^2_{\Phi_b}$ and the exact values for the variances of Φ_r and Φ_f (see eq. (13) and (16)) leads to the same conclusions that p_0 should be kept as low as possible and ϕ_0 as short as possible to minimize the effects of the OOK modulation. In order to validate this result, we have performed some simulations and measurements. In a practical situation, we have to consider the natural (noise) variance of the system inherent to the complete system, even for a non modulated carrier (perfect case with no blank periods). This noise originates from the quartz jitter, rotation jitter, etc, and, to a larger extend, from the receiver jitter at the $0 \rightarrow 1$ and $1 \rightarrow 0$ transitions. The variance of Φ_b computed theoretically can be seen as the power of additional noise induced by the OOK modulation. From a theoretical point of view, it is correct to consider that both noise are independent and therefore that the total variance is the sum of the natural noise and the noise induced by the codes.

5.1 Measurements for different codes

In our tests, we measured the variance of the beacon angular position estimator Φ_b for different codes and fields of view. The codes used are the code 0 (non modulated carrier) to compute the natural variance of the system and three variations of code 5 with increasing blank durations ("111110111110", "111110011111100", "1111100011111000"). The three last codes have a zero symbol probability p_0 equal to respectively: $1/6$, $2/7$, and $3/8$, and a blank angle ϕ_0 equal to respectively 19.25, 38.5, and 57.75 angle units (one angle unit represents $\frac{360}{62400} = 0.00577\,[degree]$). In the following, these codes are referred to, respectively, as $C0$, $C5a$, $C5b$, and $C5c$ (details about codes may be found in [3]).

5.2 Modifying the angle of view

The field of view can be modified by changing the distance between the beacon and the receiver or by changing the beacon emitted power. For practical reasons, we choose, in our experiments, to modify the emitted power, for a fixed working distance, but we will plot the measures with respect to the field of view because the value of the emitted power has no particular relevance in this study; the receiver has only access to the field of view via the demodulated signal and it is not capable to know if the distance or the power have been modified. For each code, fifty different emitted power values were chosen ranging from about $3\,[mW]$ to $150\,[mW]$ to get an approximately linear increase of the field of view (these power values/fields of view are practical values encountered in our setup). For each code and power value, 1000 angle measurements are taken to compute the variance of Φ_b. The field of view ϕ_w is defined as $\phi_f - \phi_r$. An estimator of the field of view is given by

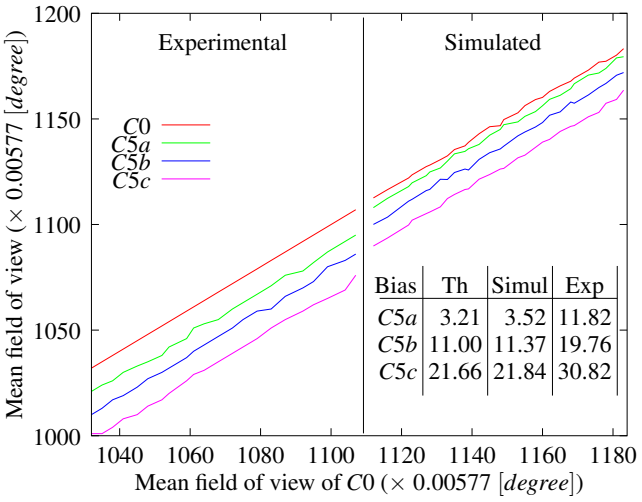

Bias	Th	Simul	Exp
$C5a$	3.21	3.52	11.82
$C5b$	11.00	11.37	19.76
$C5c$	21.66	21.84	30.82

Figure 4: Mean values of the field of view at the receiver: experimental values (left-hand side) and simulated values (right-hand side). The table provides, respectively, the theoretical, simulated, and experimental fields of view biases for $C5a$, $C5b$ and $C5c$.

$$\Phi_w = \Phi_f - \Phi_r. \tag{24}$$

The mean of Φ_w is equal to

$$\begin{aligned} \mu_{\Phi_w} &= E\{\Phi_f\} - E\{\Phi_r\}, \\ &= \left(\phi_f - p_0\frac{\phi_0}{2}\right) - \left(\phi_r + p_0\frac{\phi_0}{2}\right), \\ &= \phi_w - p_0\phi_0. \end{aligned} \tag{25}$$

As can be seen, the mean of Φ_w has a bias given by $-p_0\phi_0$. Therefore, the fields of view used to plot the data are the means of the fields of view measured for $C0$, for each power value (since the bias is null for $C0$ as $p_0 = 0$). The fields of view are shown in Figure 4 (left-hand side). The curves are linear as expected but the biases observed in the fields of view are larger than the theoretical biases (the values are given in the table of Figure 4). However they increase with p_0 and ϕ_0 as predicted, and the increments between the experimental biases are consistent with the theory.

5.3 Simulator

We developed a simulator to evaluate our theory. The three parameters considered by the simulator are the coding scheme (symbols and durations), the turret period, and the field of view. The code and the turret period are known precisely in our experiments. However, to match the reality, the simulator fields of view and natural variance were extracted from the experimental measurements of $C0$. Simulated and experimental results are thus fully comparable. The simulated fields of view and variances are presented respectively in Figure 4 (right-hand side) and Figure 5 (left-hand side). Simulations confirm our theoretical results as bounds on variances correspond to predicted bounds and the fields of view have a bias almost equal to values predicted by eq. (25) (the numerical values are given in the table included in Figure 4).

5.4 Measurements of Φ_b

The variances of the measurements are shown in Figure 5 (right-hand side). The upper bound for each code is computed after eq.

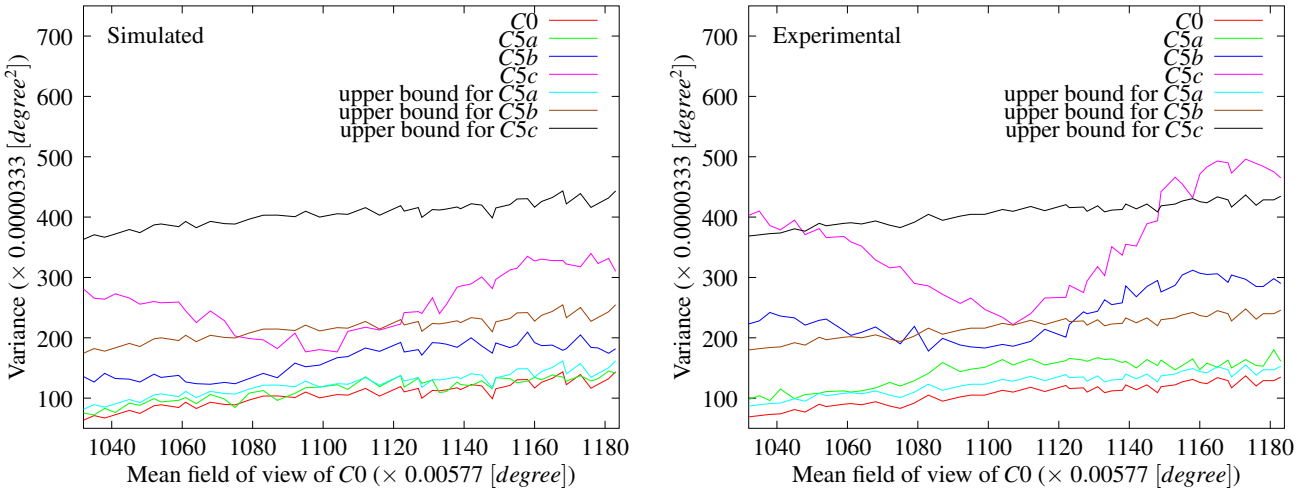

Figure 5: Variance values of the beacon angular position: simulated values (left-hand side) and experimental values (right-hand side).

(13) and added to the natural variance (derived from code $C0$) for each power value. From Figure 5, one can see that the variances are close but not always smaller than the corresponding predicted bounds for each power values, especially for $C5a$.

The slight discrepancy between the experimental results and theoretical bound means that one or more hypotheses about the system or the variance calculus are incorrect. But which ones? Our simulator provides values for the variances and biases of the field of view that matches our theory. This tends to confirm our major assumptions for the simulator (and the theory), which are: (1) the natural variance is independent of the variance added by a code and (2) the natural variance is the same whatever the code used. However, a detailed analysis of the receiver hardware shows the presence of an "Automatic Gain Control" (AGC) loop between the input and the demodulator. Typically, the gain is set to a high value when no signal is present for a "long time", resulting in a very noisy first transition (Φ_r in our case). This gain then decreases over time, resulting in sharper transitions (especially the last one, Φ_f in our case). This characteristic is clearly identifiable from the variance of Φ_r and Φ_f for a non modulated signal ($C0$). Indeed, for $C0$, the variance of Φ_r stretches from about 250 to 500 whereas the variance of Φ_f stretches from about 7 to 20. It appears that the gain value depends on the past values of the received signal and the duration of blank periods, and this produces a non constant natural variance over time. If the natural variance evolves over time, we have to consider this effect to tighten the agreement between theoretical and practical results. But it is not trivial to consider this effect because it relates to the hardware used. Finally, note that despite that evolutions of both Φ_r and Φ_f variance are quasi linear, the curve of Φ_b is not linear with respect to the field of view. This confirms that there exists a dependency between Φ_r and Φ_f (this effect is most visible for the $C5c$ curve).

6. CONCLUSIONS

This paper analyzes the errors on the measured angles of a positioning system described in [3]; one of the main issues is that it uses an On-Off Keying modulation mechanism. We propose a statistical estimator for the angular localization of a beacon and show that this estimator is unbiased and that its variance is theoretically upper bounded by $p_0\frac{\phi_0^2}{3} - p_0^2\frac{\phi_0^2}{4}$. This variance represents the power noise due to the OOK modulation; it increases with the blank angle ϕ_0 and with the proportion of zero symbols in a code p_0 (if $p_0 < \frac{2}{3}$). This study also justifies some practical choices made in [3], in particular: (1) the building of a symmetric optical part, (2) the reduction of p_0 versus p_1, and (3) the reduction of T_0 (or equivalently ϕ_0).

In the second part of this paper, we present experimental results for the variance of the beacon position due to the OOK modulation and also present the framework of a simulator that was developed to evaluate our theory. The results of the simulator are coherent with our theoretical results, but experimental results are slightly different. Experimental results enlighten that the natural variance of the system depends on the code used because of the Automatic Gain Control loop of the receiver, explaining why the experimental results do not match the theoretical bounds exactly. Whereas the experimental and simulated results differ a little, their general shape are the same, meaning that this theory seems coherent. In a practical situation, we want to limit the variance added by the codes against the natural variance of the system. The theoretical bound computed in this paper as well as the simulator may help this purpose. Note that our system achieves a remarkably low noise level on angles. Experimental values encountered in our system for the standard deviation of Φ_b range from 0.056 to 0.078 $[degree]$.

This study supposes the robot does not move during measurement. Indeed, the robot has to stop from time to time to perform some specific tasks (like grab a ball for example). We can take advantage of this situation to get better estimates of the angles to give to the triangulation calculus. If the robot moves, the estimated value for the beacon angular position has an additional error because the robot position has changed during the measurement. This has no real impact on the performance because the acquisition duration for the measurement is small compared to the robot speed (a typical acquisition duration is 2 $[ms]$, which represents a displacement of 2 $[mm]$ if the robot moves at 1 $[m/s]$). However, in our positioning system, we take this additional error into account by increasing the variance with a value proportional to the robot speed.

REFERENCES

[1] M. Betke and L. Gurvits. Mobile robot localization using landmarks. *IEEE Transactions on Robotics and Automation*, 13(2):251–263, April 1997.

[2] A. Papoulis. *Probability, random variables, and stochastic processes*. McGraw-Hill, 1991.

[3] V. Pierlot and M. Van Droogenbroeck. A simple and low cost angle measurement system for mobile robot positioning. In *Workshop on Circuits, Systems and Signal Processing (ProRISC)*, pages 251–254, Veldhoven, The Netherlands, November 2009.

[4] V. Pierlot, M. Van Droogenbroeck, and M. Urbin-Choffray. A new three object triangulation algorithm based on the power center of three circles. In *Eurobot Conference*, page 14, Prague, Czech Republic, June 2011.